Lawrence Berkeley National Laboratory
LBL Publications

Title
Numerical Modelling Analysis of Borehole Electromagnetic Methods for Imaging Serpentinized Zones During Stimulated Geological Hydrogen Production

Permalink
https://escholarship.org/uc/item/3qm6795v

Journal
Geophysical Prospecting, 74(8)

ISSN
0016-8025

Authors
Um, Evan Schankee
Alumbaugh, David
Zhang, Mengli
et al.

Publication Date
2026-10-01

DOI
10.1111/1365-2478.70263

Peer reviewed

eScholarship.org Powered by the California Digital Library
University of California

Title: Numerical Modeling Analysis of Borehole Electromagnetic Methods for Imaging Serpentinized Zones During Stimulated Geological Hydrogen Production

List of Authors:

Evan Schankee Um, Earth and Environmental Sciences, Lawrence Berkeley National Laboratory, Berkeley, CA, USA, esum@lbl.gov

David Alumbaugh, Earth and Environmental Sciences, Lawrence Berkeley National Laboratory, Berkeley, CA, USA, dlalumbaugh@lbl.gov

Mengli Zhang, Currently Department of Geology, University of Georgia, Athens, GA, USA, mengli.zhang@uga.edu; Formerly, Department of Geophysics, Colorado School of Mines, Golden, CO, USA.

Joseph Capriotti, Department of Geophysics, Colorado School of Mines, Golden, CO, USA, jcapriot@mines.edu

Noah Perkovich, Department of Geophysics, Colorado School of Mines, Golden, CO, USA, nperkovich@mines.edu

Yaoguo Li, Department of Geophysics, Colorado School of Mines, Golden, CO, USA, ygli@mines.edu

Conflict of Interest Statement: The authors declare that they have no conflict of interest influencing the research described in this manuscript.

Acknowledgements

This research was supported by the grant "Geophysical characterization and site-scale real-time monitoring in stimulated hydrogen" from Advanced Research Projects Agency-Energy (ARPA-E) of U.S. Department of Energy. The authors thank Dr. Kerry Key of BlueGreen Geophysics for their open-source EM modeling code, MARE2DEM. This research used the Lawrencium computational cluster resource provided by the IT Division at the Lawrence Berkeley National Laboratory (Supported by the Director, Office of Science, Office of Basic Energy Sciences, of the U.S. Department of Energy under Contract No. DE-AC02-05CH11231).

Abstract

The exploration and stimulation of geological hydrogen within ultramafic rocks represent an emerging frontier in energy resources. Stimulating hydrogen production involves injecting water and catalysts to accelerate serpentinization, a mineral alteration process that significantly reduces the electrical resistivity of the host rock often by several orders of magnitudes while altering other geophysical properties. Monitoring the spatial and temporal evolution of these serpentinized zones is essential for optimizing fluid flow, tracking fracture propagation, and maximizing hydrogen yields. In this study, we numerically evaluate the feasibility of two inductive borehole electromagnetic (EM) techniques, specifically cross-well and borehole-to-surface EM configurations utilizing magnetic sources and receivers, for imaging the electrical resistivity changes associated with induced serpentinization. We construct time-lapse subsurface electrical resistivity models representing varying degrees of serpentinization over time within a

crystalline basement overlain by a conductive sedimentary cover. We simulate forward responses and perform inversions to assess the resolving power of each EM method. Our numerical inversion results demonstrate that cross-well EM methods, operating at a high source frequency of 10,000 Hz, provide comprehensive tomographic coverage and accurately image the geometry and resistivity of the 20 to 30 meter thick serpentinized zones even during the early stages of stimulation. In contrast, the borehole-to-surface EM approach requires lower source frequencies of 1,000 Hz to ensure the EM energy penetrates the conductive overburden, which makes it less sensitive to thin, early-stage serpentinized zones. However, as the stimulated zone expands to 60 to 80 meters in thickness over time, the borehole-to-surface EM method successfully delineates the broader serpentinized volume. We conclude that cross-well EM monitoring is the preferred high-resolution tool when multiple wells are available, whereas borehole-to-surface EM monitoring remains a practical alternative in single-well scenarios during advanced stages of stimulation.

Key Words: Electromagnetics, Borehole geophysics, Inversion, Monitoring and Numerical study

Data Availability Statement: The modeling data supporting the findings of this study are available from the corresponding author upon reasonable request.

1. Introduction

Natural geological hydrogen, also termed gold hydrogen, refers to molecular hydrogen that forms and accumulates within the Earth's crust through natural geological processes (Hand, 2023). It has been identified in a variety of subsurface settings, frequently associated with rock types capable of generating hydrogen over geological timescales. One of the principal formation mechanisms is serpentinization, in which olivine- and pyroxene-rich rocks (i.e., ultramafic rocks) react with water to produce serpentine minerals, magnetite, and molecular hydrogen (McCollom et al., 2022; Milkov, 2022). Once considered rare, geological hydrogen is now thought to be more widespread (Hand, 2023), suggesting the potential for significant subsurface accumulations if the distribution of hydrogen-producing source rocks can be delineated and effective geophysical exploration strategies can be formulated (Meju and Saleh 2023; Zhang and Li, 2024; Li and Zhang, 2025; Zhang et al., 2025).

In addition to gold hydrogen exploration, there is growing interest in stimulating hydrogen source rocks and producing hydrogen. Hydrogen generated through such stimulation is termed 'orange hydrogen'. Figure 1 illustrates the process: water and catalytic additives are injected into hydrogen source rocks to induce accelerated serpentinization and generate hydrogen (Hand, 2023; Capriotti et al., 2024; Zhang and Li, 2025; Mathur et al., 2025). Laboratory experiments (McCollom and Bach, 2009; Larson et al., 2025) show that Fe-rich ultramafic rocks can produce hydrogen at temperatures below 100 °C and that production rates are highly sensitive to fluid chemistry, dissolved-gas composition, and mineral-catalyst additions that control water–rock interactions. In practice, successful implementation requires detailed knowledge of the

distribution, composition, and reactivity of hydrogen source rocks to design effective stimulation strategies.

Serpentinization can significantly change geophysical properties of hydrogen source rocks. For example, seismic velocities decline because the replacement of olivine and pyroxene by serpentine minerals introduces fine-scale cracks, increases pore space, and substitutes high-velocity minerals with lower-velocity alteration products (Mathur et al., 2025). Bulk rock density is reduced because serpentine minerals have lower intrinsic density than the original ultramafic minerals, and the hydration reaction expands the rock volume (Li and Zhang, 2025). Serpentinization also changes the electrical and magnetic properties of hydrogen source rocks. Electrical resistivity decreases because serpentinization produces magnetite and interconnected fluid-filled microfractures that create effective conductive pathways (Mathur et al., 2025). For example, serpentinization can reduce the electrical resistivity of ultramafic rocks by several orders of magnitude (Cutts et al., 2021; Capriotti et al., 2024). Magnetic susceptibility increases because magnetite generated by serpentinization is strongly magnetic compared to the primary silicate minerals it replaces (Li and Zhang, 2025). These changes within hydrogen source rocks allow geophysical methods to detect, image, and characterize serpentinization as hydraulic stimulation progresses.

To effectively stimulate hydrogen source rocks, it is necessary to understand how fractures propagate through hydrogen source rocks, where injected water flows, which portions of the rocks have already undergone serpentinization, and which areas still require further alteration. These processes can be carefully examined with borehole geophysics by placing geophysical sensors in a well close to the stimulated zone and measuring time-lapse changes in geophysical responses

produced by fracturing, fluid movement, and serpentinization. Furthermore, since stimulation and serpentinization can affect several physical properties as mentioned earlier, multiple geophysical methods and/or multiphysics approaches can be considered (Zhang and Li, 2024; Li and Zhang, 2025).

In this study, we focus on two borehole electromagnetic (EM) techniques: cross-well EM (Alumbaugh and Morrison, 1995; Wilt et al., 1995) and borehole-to-surface EM (Miura et al., 1996; Tseng et al., 1998). To the best of the authors' knowledge, the two methods have not appeared in geophysical literature for the purpose of monitoring geological hydrogen production. Although they are established tools for monitoring hydrocarbon reservoirs and CO_2 storage (Wilt and Schenkel, 1992; Marsala et al., 2007; Pardo et al., 2008; Rahmani et al., 2015; Um et al., 2020), these conventional applications are typically restricted to relatively conductive sedimentary rock formations. In contrast, as will be demonstrated in our models, stimulated hydrogen production occurs in highly resistive ultramafic host rocks (often >10,000 ohm-m), where active serpentinization induces a multi-order-of-magnitude drop in resistivity. Because this highly resistive background and large anomaly contrast represent a vastly different parameter range compared to typical fluid-substitution scenarios in sedimentary formations, the feasibility of EM monitoring in this specific context remains to be established. Accordingly, we numerically evaluate cross-well EM and borehole-to-surface EM methods for their abilities to image resistivity changes caused by ongoing stimulation-induced serpentinization.

This paper is organized as follows. We first present a set of time-lapse subsurface models that represent stimulated hydrogen production through time. By converting the conceptual serpentinization models into corresponding electrical resistivity models, we aim to provide a

benchmark modeling framework for the geophysics community to test future monitoring survey designs. Based on the electrical resistivity structures of these test models, we discuss candidate EM geophysical tools for monitoring serpentinization, including the rationale for our choices. Using the models, we then numerically evaluate cross-well EM and borehole-to-surface EM for imaging serpentinized zones. The goal of this numerical modeling study is to assess their feasibility as high-resolution imaging and monitoring tools for stimulated geological hydrogen production.

2. Conceptual Serpentinization Model and Associated Electrical Conductivity Model

A background model (Figure 2a) for the conceptual serpentinization models used in this study represents a shallow crystalline basement overlain by a sedimentary cover. The crystalline basement is assumed to be ultramafic dominated (peridotite/dunite analog), representing hydrogen source rock. In this setting, we assume the naturally occurring alteration mechanism is serpentinization caused by downward infiltrating meteoric water and the water causes variable degree serpentinization reaction. In this idealized setting, the degree of alteration should diminish with depth.

The vertical structure of the baseline state (Figure 2a) of the source rock with naturally occurring serpentinization is prescribed as follows. The upper 0–100 m of the model corresponds to the sedimentary cover. The crystalline basement begins at 100 m depth and initially consists of a transitional zone in which serpentinization decreases downward from strongly altered conditions at the basement surface to weaker alteration by 250-m depth. Between 250 and 500 m,

the basement is weakly altered. Below 500 m, the ultramafic rock is assumed to be fresh and unaltered. These assumptions of depths are based on the lithology change observed from one of borehole in Oman drilling project (Keleman et al., 2017).

We also assume that the degree of serpentinization is the primary control on bulk resistivity changes in the source rock that is undergoing serpentinization. Resistivity is expected to decrease with increased serpentinization alteration due to the increase in free water content. We adopt a log linear relationship between serpentinization fraction and resistivity based on lab measurements for dunite samples of various alteration degrees reported in He et al. (2018). The simple interpolator can be expressed as: $\rho(S)=\rho_f\left(\frac{\rho_a}{\rho_f}\right)^S$, where ρ_f is the resistivity of fresh, unaltered ultramafic rock and ρ_a is the resistivity of highly altered, serpentinized rock. The serpentinization fraction S varies between 0 and 1. Values derived from He et al. (2018) correspond to $\log_{10}$ resistivity values of 5.5 for fresh rock and 1.6 for highly serpentinized rock, yielding roughly a 4 order of magnitude range. This relationship is used to describe the resistivity in the basement. This overburden is assigned to a homogeneous low resistivity of 30 Ωm.

Fresher source rock near the bottom of the natural alteration transition will be a favorable target for stimulation efforts in stimulated geologic hydrogen production. Accordingly, we experiment with a scenario in which a horizontal well is placed at 300-m depth with three discrete injection points along its length as shown in Figure 2. We assume that water with the appropriate temperature is injected into such source rock unit to artificially stimulate serpentinization for hydrogen gas production.

Following the conceptual approach of Capriotti et al. (2025), ellipsoidal volumes centered on these injection points represent volumes of stimulated serpentinization (Figures 2b and 2c). In these volumes, the serpentinization degree is set to 80%, which modifies the resistivity values in these zones using the above-described relationship. Outside these stimulated zones, the background alteration structure remains unchanged. Thus, the time-lapse resistivity models consist of a baseline model corresponding to the assumed natural state of the serpentinization in the ultramafic basement rock (T0; Figure 2a) and the two additional resistivity models (T1 and T2; Figures 2b and 2c) corresponding to different states following the initiation of stimulated serpentinization.

3. Borehole Electromagnetic Geophysics

The stimulated hydrogen production models show significant changes in electrical resistivity over time because of ongoing serpentinization. At time T1, the resistivities of the three stimulated zones decrease by roughly two orders of magnitude at a depth of 300 m. At time T2, the zone thickness increases from 20–30 m to 60–80 m, and the width expands from a few hundred meters to more than one kilometer. Consequently, one could consider using surface controlled-source EM methods or high-frequency magnetotelluric methods to image the stimulated zones. A major obstacle for the surface EM approaches, however, is the presence of thick, conductive overburden that prevents the use of high-frequency controlled- or natural-source EM fields, because such EM signals would be strongly attenuated through the conductive overburden before reaching the 300 m target depth. As a result, surface EM would need to be operated at suboptimal frequencies in

this environment, leading to low-resolution imaging results that are not ideally suited for geophysical monitoring.

In this environment, borehole EM methods can be effective, especially when wells already exist (Figures 1 and 2) and are either chrome-cased or left open for magnetic-field measurements. For example, in cross-well EM (Alumbaugh et al., 1995; Wilt et al., 1995), a magnetic dipole source is deployed in one well and a magnetic receiver in the other. Because both the source and receiver can be positioned below the top conductive layer, a high source frequency can be selected without that layer's influence. Magnetic fields are measured with the source–receiver pair at many different positions, and inversion of the cross-well EM data can provide high-resolution resistivity images between the two wells.

When only one well is available, borehole-to-surface (or surface-to-borehole) EM methods can be employed by placing a receiver (or source) in the well and a source (or receiver) on the surface, and these methods can use either electric or magnetic sources and receivers. For our time-lapse models (Figure 2) we use a magnetic source- magnetic receiver configuration because the target is conductive and magnetic-field measurements are less sensitive to seasonal near-surface inhomogeneities that complicate data interpretation in practice. We use a vertical magnetic loop source on the surface and a vertical magnetic receiver in the borehole. Borehole-to-surface EM often uses lower source frequencies than cross-well EM because its source-receiver separation is generally larger than that in cross-well EM, making lower frequencies more suitable. In our models, these lower frequencies also ensure that the surface EM fields remain detectable after passing through the conductive overburden.

It is also worth noting that the downhole casing-source EM method (Marsala et al., 2014; Tang et al., 2015; Puzyrev et al, 2017; Um et al., 2020; MacLennan, 2022) could be a good candidate for imaging the serpentinized zone. In this configuration, one electrode is connected to the steel-cased well near the stimulated zone and the other electrode is grounded at the surface, which allows the casing to act as an enhanced vertical source while EM fields are measured on the surface. This method has been used to image and monitor CO_2 plumes at enhanced oil recovery sites (MacLennan, 2022) and to characterize fluids and fractures at enhanced geothermal systems (Um et al., 2024). This method could also work well for the serpentinized zone described earlier. However, our preliminary numerical modeling has revealed that numerical instabilities arise from the large resistivity contrast created by inserting a highly conductive steel casing (~$5 \cdot 10^6$ S/m) into very resistive unaltered ultramafic rock (~$3 \cdot 10^{-6}$ S/m), as well as from the large cell-size contrast needed to discretize the thin hollow casing with fine cells (mm scale) while using larger cells (a few hundred meter scale) for other subsurface regions. Modeling EM interactions among multiple cased wells also introduces further numerical challenges (Alumbaugh et al., 2025). We think the casing-source EM method holds promise for monitoring a serpentinized zone, but addressing the associated numerical challenges remains an active area of ongoing research, and we do not pursue its application here.

Serpentinization also increases magnetic susceptibility from 0 to 0.03~0.05 (Capriotti et al., 2025). However, at source frequencies between a few thousand and ten thousand Hz, the responses of both cross-well and borehole-to-surface EM methods show little sensitivity to susceptibility changes of this magnitude. In the kHz frequency band used for cross-well EM, the fields are in the diffusion domain and the governing equation is $\nabla^2 H = j\omega\mu\sigma H$, where H is the

magnetic field, ω is the angular frequency, μ is the magnetic permeability, and σ is the electrical conductivity. The data therefore depend on the product μσ. Therefore, when serpentinization results in such changes in the magnetic susceptibility, the resulting small perturbation in the parameter is easily masked by the large changes in electrical conductivity that result from serpentinization, as well as by uncertainties from noise, imprecise source-receiver positions, and borehole deviation. Therefore, we have not considered changes in magnetic susceptibility due to serpentinization in our modeling studies.

As a side note, such localized changes in magnetic susceptibility due to serpentinization can be detected by the DC or low-frequency cross-well magnetic method (Capriotti et al., 2025). In the magnetostatic domain, the measured magnetic field depends directly on the magnetic susceptibility of the medium. Even a small change in susceptibility from 0 to 0.05 induces a proportional change in the static magnetic field, in a way that is not masked by conductive or displacement current effects. Thus, the method can resolve subtle susceptibility variations that would be negligible in borehole EM measurements. Nonetheless, the magnetic method is based on a potential equation, and does not provide the level of imaging resolution provided by borehole EM methods for monitoring purposes, as will be demonstrated in the next section.

4. Forward and Inverse Modeling Studies

Figure 3 shows a cross-well EM configuration within the three models we are investigating with a dense, uniform receiver spacing, superimposed on the time-lapse electrical resistivity models. Magnetic receivers are placed every 10 m from z = 100 m to z = 500 m along the two monitoring

wells located at x = −500 m and x = 500 m. This arrangement implies that the cross-well EM experiment has a vertical resolution on the order of 10 m, which is appropriate because the serpentinized zones in the time-lapse models range from 20 m to 80 m in thickness. A vertical magnetic source is positioned in the well at x = 0 m and is moved from z = 100 m to z = 500 m. For numerical implementation, we simulate a cross-well EM source at 10,000 Hz at discrete 10 m intervals rather than simulating continuous motion although in practice, we use the magnetic-field data averaged over each 10 m depth interval.

For all EM forward and inverse modeling experiments in this study, we utilize MARE2DEM (Key, 2016), a 2.5-D adaptive mesh finite element EM code. Two of its key features make it particularly suited for this application: goal-oriented adaptive mesh refinement and the use of a sparse direct solver. The adaptive meshing automatically refines the computational grid around the thin stimulation zones and borehole sensor locations, ensuring highly accurate EM responses without requiring manual grid design. Furthermore, because our geological hydrogen models feature a large range of electrical resistivity values, spanning the highly resistive ultramafic background and the highly conductive stimulated zones, matrix conditioning can become challenging for EM modeling algorithms that use iterative solvers. Such solvers may require careful preconditioning to achieve reliable convergence in these petrophysical environments. While preconditioning might be successfully tuned for a few individual forward simulations, it is difficult to guarantee robust convergence across the many dynamically evolving resistivity models required throughout the course of an inversion. By employing direct matrix factorization, MARE2DEM robustly computes the EM fields across these large resistivity contrasts, providing

a numerically stable solution without the conditioning challenges posed by large resistivity variations in these models.

Regarding the dimensionality of the simulations, while the conceptual serpentinization models represent 3D geological structures, the 2.5D modeling approach approximates the geology as 2D while computing 3D EM fields. This approximation is highly applicable to cross-well EM because the method fundamentally operates as a 2D imaging tool on the plane defined by the source and receiver wells. Borehole-to-surface EM, however, can be more sensitive to off-plane 3D geometries, especially if multiple surface source lines are deployed radially around the well. Additionally, replacing a finite 3D stimulated zone with a 2D counterpart assumes the anomaly has an infinite strike length. This lack of finite boundaries generally produces stronger EM responses than a true 3D body. To mitigate these geometric effects and ensure the 2.5D approximation remains reasonable for our borehole-to-surface EM analysis, we restricted our model setup to a single surface source profile with zero offset from the 2D imaging plane. Even with this restriction, it should be noted that the 2.5D approach to the borehole-to-surface EM may represent a slightly optimistic scenario for target detectability compared to a highly localized 3D field setting.

Figure 4 shows simulated cross-well EM amplitude and phase data for the baseline resistivity model (T0) and two subsequent models (T1 and T2). Measurable differences in both amplitude and phase are observed as shown in Figure 4. These differences become clearer when the relative differences in amplitude and phase between T0 and T1 or T2 are calculated, as shown in Figure 5. For example, measurable differences (> 5-10 % in amplitude and > 5–10° in phase) occur in the central region of the difference maps.

For the inversion experiments, we use the layered resistivity model prior to stimulation (T0) as a starting model. The active inversion domain is restricted to the region below 200 m depth. Because the approximate depth and volume of the stimulated zone are generally known during such operations, the shallower, unaffected regions are excluded from the inversion updates and kept fixed. This restriction of the inversion domain produces the distinct horizontal boundary observed at 200 m depth in the inverted models as will be shown. Based on our recent cross-well EM data acquisition and interpretation (Um et al., 2020b), the cross-well EM data for T1 and T2 are contaminated with noise equal to 2% of their amplitude and phase. Then, the data are weighted using a noise floor defined as 1% of the peak amplitude of the common receiver gather to which each data point belongs. All synthetic data amplitudes are larger than the noise floor of a typical induction coil receiver (e.g., 0.01 pT), and thus all data points are retained for the inversion. The inversions successfully converged to a data misfit of approximately 1.0.

The right column of Figure 3 presents the resulting cross-well EM inversion results. At the early stage of stimulation (T1), when the stimulated zone is thin, the inversion (Figure 3a) captures the overall boundaries of the zone, although some imaging artifacts are shown. For example, the recovered resistivities inside the stimulated zone are slightly lower than the true values, and the recovered zone is somewhat horizontally discontinuous. These imaging artifacts are related to the survey aspect ratio, which is defined as the ratio of vertical coverage to well spacing. A larger aspect ratio generally yields better horizontal imaging resolution and can mitigate these artifacts. However, in practice, the spacing between injection and production wells is typically a fixed parameter for cross-well EM survey design (unless dedicated monitoring wells are prepared for

cross-well EM), and the vertical coverage is also constrained by well depth and the top conductive layers.

At the later stage (T2), when the stimulated zone becomes thicker and wider, the inversion more accurately delineates the zone in both resistivity and geometry (Figure 3c). The recovered conductive features are more horizontally continuous, and the resistivity values are closer to the true ones than those from the T1 inversion (Figures 3a). We repeated the cross-well inversion for the other yz cross-sections (Figures 3b and 3d) and obtained similar results. After time T1, the inversion outlines the general geometry of the serpentinized zone but underestimates its resistivity and shows horizontal discontinuities, whereas after time T2, the inversion better recovers the thicker, wider zone. Overall, the inverse modeling experiments show that the method has sufficient capability for imaging the spatial distribution of the serpentinized zone over time.

Next, we examine the borehole-to-surface EM responses simulated using the same three models (T0, T1, and T2). In this configuration, magnetic receivers are placed on the surface while the vertical magnetic source moves from 100 m to 500 m in depth. A 2km long surface magnetic field profile is covered using magnetic receivers with 20m spacing, while the receiver spacing was 10m in the cross-well EM. Due to the thick, conductive overburden, the source frequency for the borehole-to-surface EM method was set to 1,000 Hz, which is an order of magnitude lower than that of the cross-well EM. Figures 6 and 7 compare the surface magnetic-field amplitude and phase, along with their relative differences among the three models. As shown in Figure 6, the borehole-to-surface EM method is not sufficiently sensitive to the thin, small serpentinized zone in model T1, producing less than a 5–10% relative difference in amplitude. As a result, the relative-difference plot (Figure 6d) appears to be noise. As the serpentinized zone becomes larger

in model T2, the borehole-to-surface EM responses become sufficiently sensitive to the zone, producing larger than a 5–10% relative difference. The resulting relative differences are less noisy, larger, and more coherent. Consequently, we applied the inversion only to the data from model T2

Figure 8 shows the borehole-to-surface EM inversion results for model T2, displayed as xz and yz cross-sections. The true models in the left column of Figure 8 are the same as those in Figures 3c and 3d. However, the left column of Figure 8 displays a larger cross-sectional area of the models to accommodate the larger region imaged by the borehole-to-surface EM method compared to the cross-well EM method. Overall, the borehole-to-surface EM inversion effectively delineates the serpentinized zone's geometry and resistivity.

Thus far, we have examined the imaging capabilities of the two borehole EM methods as the injection process alters the electrical conductivities of the stimulated zones. Next, we investigate whether these imaging capabilities are influenced by background model variations. At a geological hydrogen production site, we expect multiple wells to provide electrical resistivity logs suitable for constructing a reasonably accurate background model. Nonetheless, ultramafic formations may exhibit complex geological heterogeneity that cannot be fully captured by well-log data alone. To examine the effects of such heterogeneity, we did not use the uniform layered background model (T0, Figure 2a) for this inversion experiment; instead, we randomly perturbed the resistivity of each cell in the layered model by ±10%. This perturbed model was then used as a new starting model to invert the same borehole EM data used in the previous inversion experiments.

Figure 9 compares the true models, the inversion results derived from the unperturbed layered background model, and the new inversion results derived from the perturbed background model. At T1, using the randomly perturbed starting model yields cross-well EM imaging (Figure 9a) that shows slightly more deviation from the true model (Figure 3a) than when the unperturbed layered model is used. However, at T2, as the stimulated zone becomes thicker and wider, the cross-well EM inversion recovers the geometry and resistivity of the stimulated zones just as effectively as the inversion utilizing the unperturbed starting model (Figure 9b). We draw a similar conclusion for the borehole-to-surface EM inversion, as those results are also insignificantly affected by the perturbed background model (Figure 9c)

In the modeling examples presented here, a comparison of the two borehole EM methods shows that, when both use magnetic sources and receivers, cross-well EM yields more accurate inversion results than borehole-to-surface EM for two main reasons. First, due to the model's thick, conductive top layers and large source-receiver offsets, the borehole-to-surface EM method requires a source frequency an order of magnitude lower than that used for cross-well EM. Second, cross-well EM provides superior tomographic coverage because the geometry of sources and receivers in adjacent wells generates a high density of overlapping Fresnel-like sensitivity zones, thoroughly sampling the inter-well region. In contrast, borehole-to-surface EM offers sparser tomographic coverage, as its sensitivity zones are much less overlapping while traveling from depth to the surface, yielding a less focused image (Um et al., 2020). Nonetheless, the borehole-to-surface inversion results demonstrate that the method can serve as an effective geophysical tool for monitoring the serpentinized zone when only a single well is available.

5. Conclusions and Discussion

In this study, we adapted CSM's conceptual serpentinization models to provide a benchmark computational framework for testing and optimizing monitoring survey designs around a shallow horizontal well. The first-order resistivity-serpentinization relationship used here is admittedly rudimentary, but it offers a practical starting point for the geophysics community to evaluate emerging technologies. Developing a more site-specific understanding of the relationship between serpentinization and resistivity, as well as other potential alteration processes, will be critical for refining both imaging and monitoring strategies. When such relationships become available, the model generation procedure and methodologies presented here can be readily adopted.

Using CSM's serpentinization modeling framework, our numerical studies show that borehole EM methods are effective for imaging and monitoring stimulation-induced serpentinization in hydrogen source rocks. Cross-well EM produces more accurate inversion results than borehole-to-surface EM because it operates at higher frequencies and provides more comprehensive tomographic coverage between wells. Borehole-to-surface EM is less sensitive during the early stages of stimulation but can delineate the serpentinized zone once it becomes thicker and wider. Consequently, cross-well EM is the preferred option for high-resolution monitoring when multiple wells are available, whereas borehole-to-surface EM remains a practical alternative in single-well settings.

While we have presented the numerical feasibility of these EM methods for monitoring stimulated geological hydrogen production, successfully translating these numerical demonstrations to real-world applications requires moving beyond the idealized modeling analysis. In practical field settings, ultramafic formations may exhibit geological heterogeneity,

including natural fracture networks, variable primary mineralogy, and localized zones of pre-existing serpentinization. These background resistivity variations may not be captured using a simple layered background model such as one used in this study. However, since a geological hydrogen production site typically requires multiple wells, resistivity log data can be assumed to be available to construct a reasonable background model. Our inversion experiments show that the borehole EM methods can also recover the geometry and the resistivity of the stimulated zones when the layered background model is somewhat perturbed. The time-lapse inversion can also be performed to mitigate this static geologic complexity. For example, by employing a data-difference inversion strategy, post-stimulation monitor data can be inverted using the baseline model as both a starting and reference model. Fitting the data differences between the pre- and post-stimulation surveys, rather than the absolute data, largely suppresses the influence of static background heterogeneity and isolates the resistivity changes driven by fluid flow and serpentinization.

Beyond managing geological complexity, the spatial resolution of the EM methods needs to be considered under field setting and survey costs. For cross-well EM, achieving the best results requires selecting the highest possible source frequency that still provides measurable signals at the receiver well. Once this optimal frequency is established, vertical resolution is primarily determined by the source and receiver intervals, which can be controlled during the survey, but finer intervals mean higher survey costs. In contrast, horizontal resolution is typically limited to roughly 5% of the interwell spacing. Because well spacing in field-scale projects is determined by overall hydrogen production strategies rather than being optimized solely for geophysical monitoring, the achievable horizontal resolution is inherently tied to these broader operational

constraints. A similar physical limitation applies to borehole-to-surface EM, where common conductive sedimentary overburden acts as a low-pass filter, physically restricting the method to relatively low source frequencies compared to cross-well EM and thereby limiting it to detecting broader, bulk volumetric expansion rather than localized, early-stage changes. Recognizing these operational and physical boundaries is critical for designing effective surveys.

In this study, we focused on the EM methods that employ inductive magnetic sources. However, as mentioned earlier, the casing-source EM method, which utilizes galvanic electric sources, provides another approach for detecting and imaging deep, localized stimulated zones. A major challenge in interpreting casing-source EM data at a geological hydrogen production site is the accurate and efficient simulation of steel casing effects, as steel-cased wells are ubiquitous in these environments. Hollow steel casings are typically only a few centimeters thick, yet they can be up to ten orders of magnitude more conductive than the surrounding ultramafic rocks and are magnetically permeable. Because these properties significantly distort EM data, their effects must be modeled accurately. To the best of the authors' knowledge, the development of 3D EM modeling and inversion algorithms capable of accurately and efficiently simulating a wide range of EM responses resulting from multiple steel-cased wells and complex surface steel infrastructure is still in its infancy. Advancing these computational capabilities represents an important next step because the joint use of magnetic- and electric-source EM methods will provide more comprehensive monitoring of underground geological hydrogen production.

6. References

Alumbaugh, D.L. and Morrison, H.F., (1995) Theoretical and practical considerations for crosswell electromagnetic tomography assuming a cylindrical geometry. Geophysics 60, 846-870.

Alumbaugh, D., Um, E., Moe, G., Macquet, M. and Cooper, J., (2026) Evaluation of vertical electric source time-domain electromagnetic method for monitoring subsurface carbon storage: field trials, modeling, and steel-casing effects. Geophysical Prospecting (re-submitted after minor revision).

Capriotti, J., Perkovich, N., Zhang, M. and Li, Y., (2025) Geophysical responses of stimulated hydrogen production in ultramafic rocks. International Meeting for Applied Geoscience and Energy (IMAGE) Abstract.

Cutts, J.A., Steinthorsdottir, K., Turvey, C., Dipple, G.M., Enkin, R.J. and Peacock, S.M., (2021) Deducing mineralogy of serpentinized and carbonated ultramafic rocks using physical properties with implications for carbon sequestration and subduction zone dynamics. Geochemistry, Geophysics, Geosystems 22, e2021GC009989.

Hand, E., (2023) Hidden hydrogen. Science 379, 630-636.

He, L., Chen, L., Dorji, He, Z., Wang, X., Xiao, B., Xu, L., Zhao, X., Xi, X., Yao, H. and Chen, R., (2018) Mapping chromite deposits with audio magnetotellurics in the Luobusa ophiolite of southern Tibet. Geophysics 83, B47-B57.

Kelemen, P.B., Godard, M., Johnson, K.T., Okazaki, K., Manning, C.E., Urai, J.L., Michibayashi, K., Harris, M., Coggon, J.A. and Teagle, D.A., (2017) Peridotite carbonation at the leading edge of the mantle wedge: OmDP Site BT1. AGU Fall Meeting Abstracts, V24E-06.

Key, K., (2016) MARE2DEM: a 2-D inversion code for controlled-source electromagnetic and magnetotelluric data. Geophysical Journal International 207, 571-588.

Larson, T., Ukar, E., Gelencser, O., Zhang, T. and Fall, A., (2025) Geochemical exploration techniques to quantify hydrogen generation potential in complex geologic terranes. International Meeting for Applied Geoscience and Energy (IMAGE) Abstract.

Li, Y. and Zhang, M., (2025) Geologic hydrogen exploration by imaging key hydrogen system components using multiple geophysical methods. Journal of Geophysics and Engineering 22, 952-961.

MacLennan, K., (2022) Monitoring CO2 storage using well-casing source electromagnetics. The Leading Edge 41, 107-113.

Marsala, A.F., AlRuwaili, S., Ma, S.M., Modiu, S.L., Ali, Z., Donadille, J.M. and Wilt, M., (2007) Crosswell electromagnetic tomography in Haradh field: modeling to measurements. SPE Annual Technical Conference and Exhibition, SPE-110528.

Marsala, A.F., Hibbs, A.D. and Morrison, H.F., (2014) Borehole casing sources for electromagnetic imaging of deep formations. SPE Annual Technical Conference and Exhibition, SPE-170845.

Mathur, Y., Moise, H., Aydın, Y. and Mukerji, T., (2025) Techno-economic analysis of natural and stimulated geological hydrogen. International Journal of Hydrogen Energy 165, 150872.

McCollom, T. and Bach, W., (2009) Thermodynamic constraints on hydrogen generation during serpentinization of ultramafic rocks. Geochimica et Cosmochimica Acta 73, 856-875.

McCollom, T.M., Klein, F. and Ramba, M., (2022) Hydrogen generation from serpentinization of iron-rich olivine on Mars, icy moons, and other planetary bodies. Icarus 372, 114754.

Meju, M.A. and Saleh, A.S., (2023) Using large-size three-dimensional marine electromagnetic data for the efficient combined investigation of natural hydrogen and hydrocarbon gas reservoirs: a geologically consistent and process-oriented approach with implications for carbon footprint reduction. Minerals 13, 745.

Milkov, A.V., (2022) Molecular hydrogen in surface and subsurface natural gases: abundance, origins and ideas for deliberate exploration. Earth-Science Reviews 230, 104063.

Miura, Y., Osato, K., Takasugi, S., Muraoka, H. and Yasukawa, K., (1996) Development of the vertical electro magnetic profiling (VEMP) method. Journal of Applied Geophysics 35, 191-197.

Pardo, D., Torres-Verdín, C. and Zhang, Z., (2008) Sensitivity study of borehole-to-surface and crosswell electromagnetic measurements acquired with energized steel casing to water displacement in hydrocarbon-bearing layers. Geophysics 73, F261-F268.

Puzyrev, V., Vilamajo, E., Queralt, P., Ledo, J. and Marcuello, A., (2017) Three-dimensional modeling of the casing effect in onshore controlled-source electromagnetic surveys. Surveys in Geophysics 38, 527-545.

Rahmani, A.R., Bryant, S., Huh, C., Athey, A., Ahmadian, M., Chen, J. and Wilt, M., (2015) Crosswell magnetic sensing of superparamagnetic nanoparticles for subsurface applications. SPE Journal 20, 1067-1082.

Tang, W., Li, Y., Swidinsky, A. and Liu, J., (2015) Three-dimensional controlled-source electromagnetic modelling with a well casing as a grounded source: a hybrid method of moments and finite element scheme. Geophysical Prospecting 63, 1491-1507.

Tseng, H.W., Becker, A., Wilt, M.J. and Deszcz-Pan, M., (1998) A borehole-to-surface electromagnetic survey. Geophysics 63, 1565-1572.

Um, E.S., Kim, J. and Wilt, M., (2020a) 3D borehole-to-surface and surface electromagnetic modeling and inversion in the presence of steel infrastructure. Geophysics 85, E139-E152.

Um, E., Marchesini, P., Wilt, M., Nichols, E., Alumbaugh, D., Vasco, D., Daley, T. and Key, K., (2020b) Joint use of crosswell EM and seismics for monitoring CO2 storage at the Containment and Monitoring Institute Field Site (CaMI): Baseline surveys and preliminary results. SEG International Exposition and Annual Meeting, D031S026R008.

Um, E.S., Alumbaugh, D., Capriotti, J., Wilt, M., Nichols, E., Li, Y., Kang, S. and Osato, K., (2024) 3D modeling of deep borehole electromagnetic measurements with energized casing source for fracture mapping at the Utah Frontier Observatory for Research in Geothermal Energy. Geophysical Prospecting 72, 3104-3128.

Wilt, M. and Schenkel, C., (1992) Cross-borehole electromagnetic induction for steam flooding monitoring. SEG Technical Program Expanded Abstracts, 484-487.

Wilt, M.J., Alumbaugh, D.L., Morrison, H.F., Becker, A., Lee, K.H. and Deszcz-Pan, M., (1995) Crosswell electromagnetic tomography: system design considerations and field results. Geophysics 60, 871-885.

Zhang, M. and Li, Y., (2024) The role of geophysics in geologic hydrogen resources. Journal of Geophysics and Engineering 21, 1242-1253.

Zhang, M., Cherkose, B. and Li, Y., (2025) Predicting potential geologic hydrogen reservoir locations using MT and seismic data. International Meeting for Applied Geoscience and Energy (IMAGE) Abstract.

7. Figure Captions

Figure 1. Colorado School of Mines (CSM)'s conceptual model (Zhang, M. and Li, Y., 2024) of stimulated geological hydrogen production.

Figure 2. Time-lapse conceptual stimulated hydrogen production models with varying degrees of serpentinization and the corresponding electrical resistivity models. (a) Before stimulation (T0). The model setup features a single horizontal injection well (black solid line) at a depth of 300 m and three vertical wells (white broken lines) spaced at 500 m intervals. (b) During the early stage of stimulation (T1). (c) During a later stage of stimulation (T2).

Figure 3. Cross-well EM inversion. (a) The xz cross-section at y = 0 m at T1. (b) The yz cross-section at x = 0 m at T1. (c) The xz cross-section at y = 0 m at T2. (d) The yz cross-section at x = 0 m at T2. The left column shows the true resistivity models along with the cross-well EM configuration, and the right column shows the inversion results. The white circles along the vertical line at position = 0 m indicate source positions, and the circles at positions x= -500 m and 500 m indicate receiver positions.

Figure 4. Crosswell EM forward modeling data for the xz cross-sectional models. (a) T0. (b) T1. (c) T2. The first row shows the amplitude of the vertical magnetic field (Bz) and the second row shows their phase. The source well is at the center of the model (i.e., x=0m) and the receiver well at x=500m.

Figure 5. Difference (a) between T0 and T1 model responses and (b) between T0 and T2 model responses. The first row shows the relative amplitude difference (%) of the vertical magnetic field (Bz) and the second row shows their phase difference (degree).

Figure 6. The borehole-to-surface EM amplitude data and relative difference (%) between T0, T1 and T2 models.

Figure 7. The borehole-to-surface EM phase data and difference (degree) between T0, T1 and T2 models.

Figure 8. Borehole-to-surface EM inversion. (a) The xz cross-section at y = 0 m at T2. (b) The yz cross-section at x = 0 m at T2. The left column shows the true resistivity models along with the cross-well EM configuration, and the right column shows the inversion results. The white circles along the vertical line at position = 0 m indicate source positions, and the circles on the surface indicate receiver positions.

Figure 9. Comparison of the borehole EM inversion results derived using unperturbed and perturbed layered background starting models. Columns show the true resistivity models (left), inversions using the unperturbed starting model (middle), and inversions using the randomly perturbed starting model (right). All panels display xz cross-sections at y = 0 m for (a) cross-well EM at T1, (b) cross-well EM at T2, and (c) borehole-to-surface EM at T2.

8. Figures

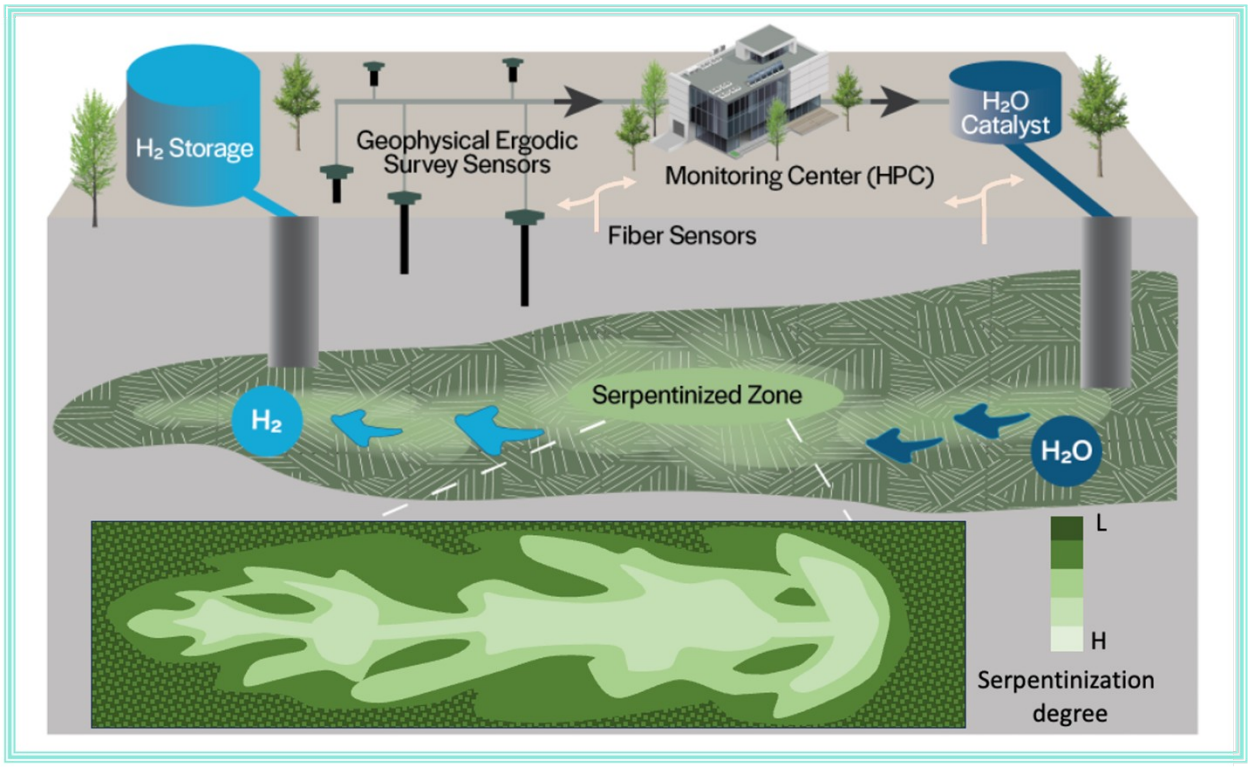
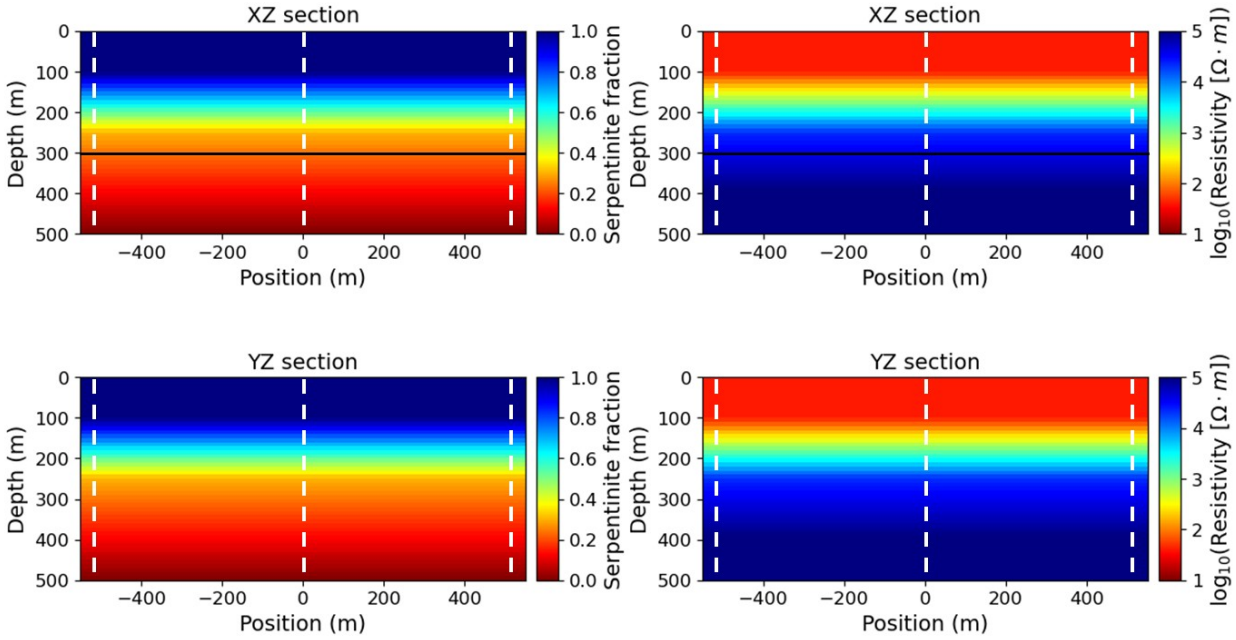
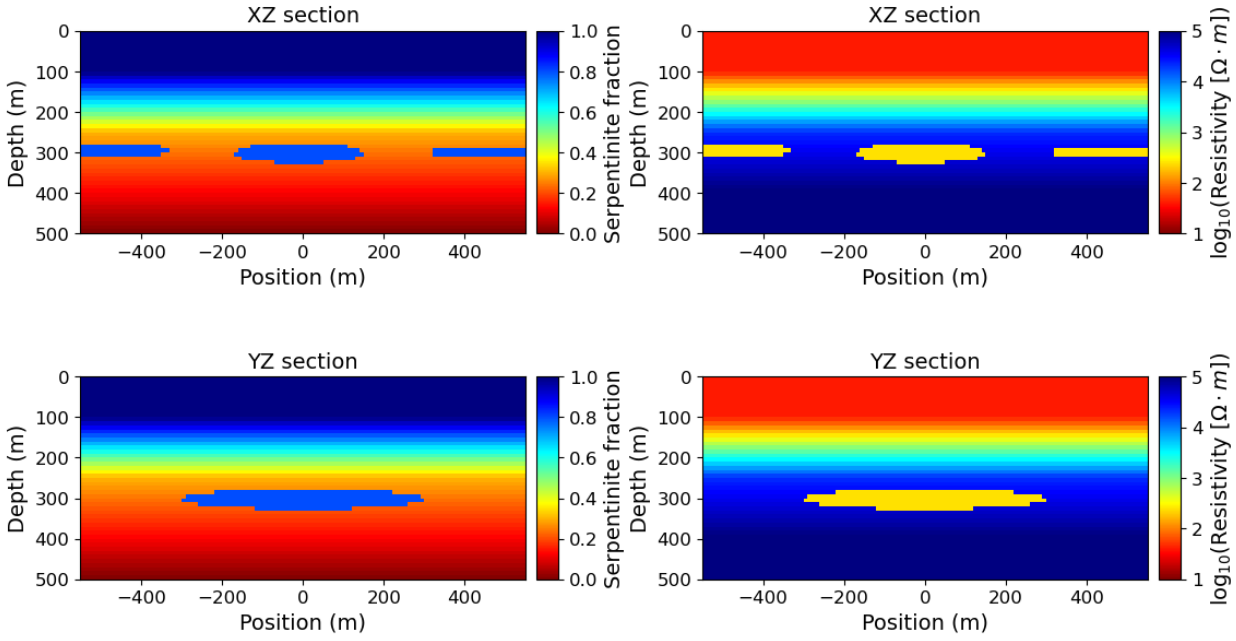


Figure 1. Colorado School of Mines (CSM)'s conceptual model (Zhang, M. and Li, Y., 2024) of stimulated geological hydrogen production.

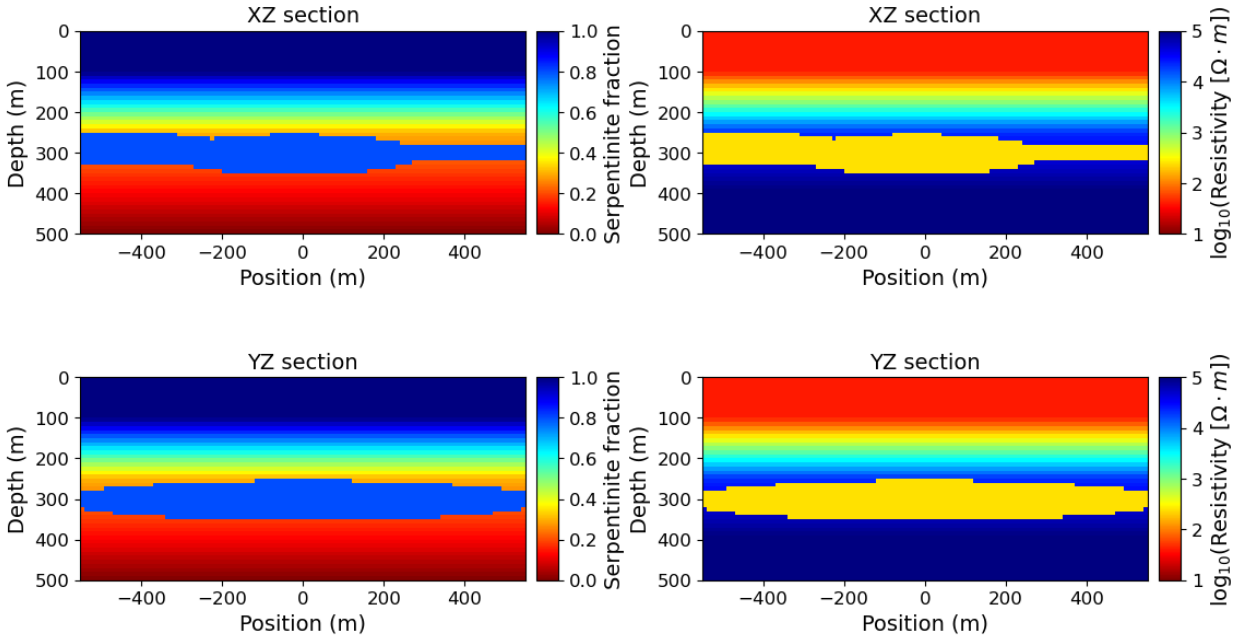


(a)



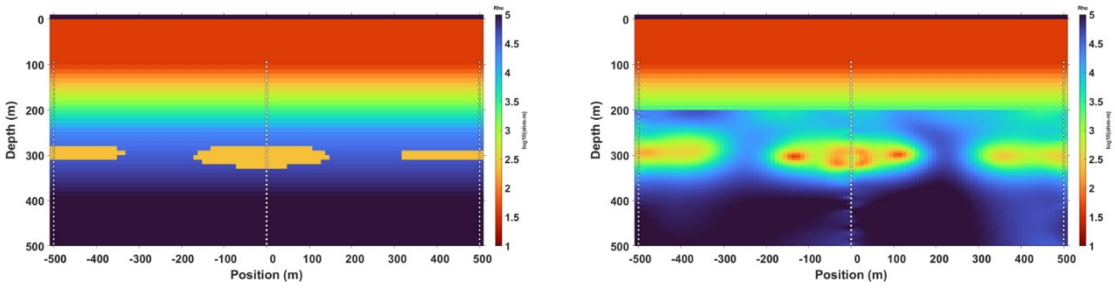
(b)

Figure 2. Time-lapse conceptual stimulated hydrogen production models with varying degrees of serpentinization and the corresponding electrical resistivity models. (a) Before stimulation (T0). The model setup features a single horizontal injection well (black solid line) at a depth of 300 m and three vertical wells (white broken lines) spaced at 500 m intervals. (b) During the early stage of stimulation (T1). (c) During a later stage of stimulation (T2).

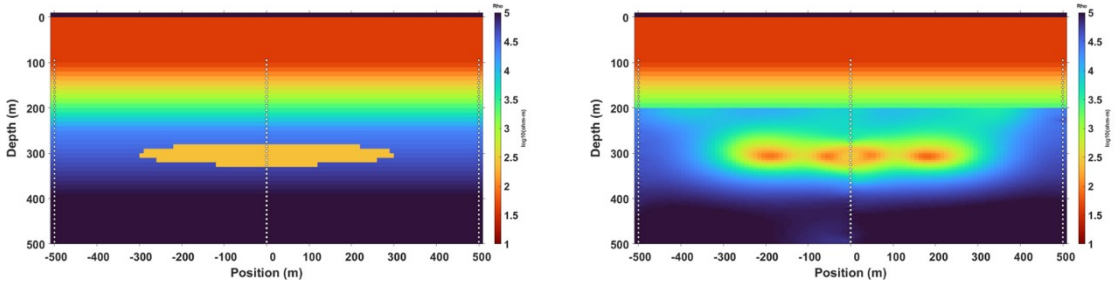


(c)

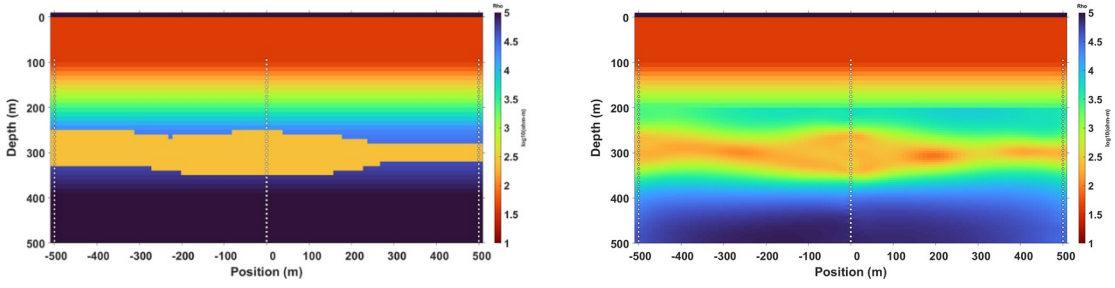
Figure 2. Continued.



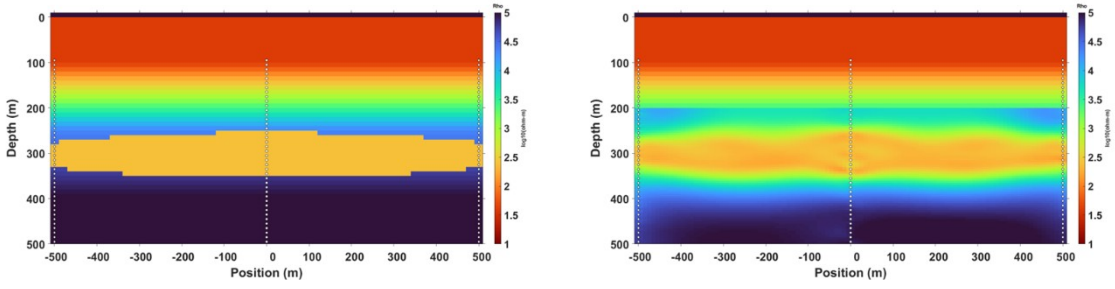
(a)



(b)



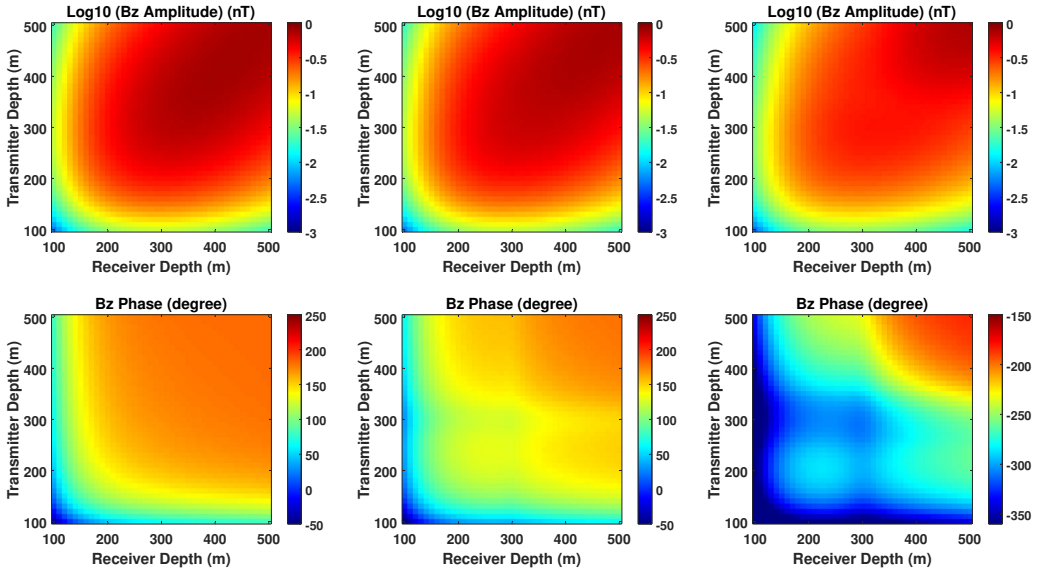
(c)



(d)

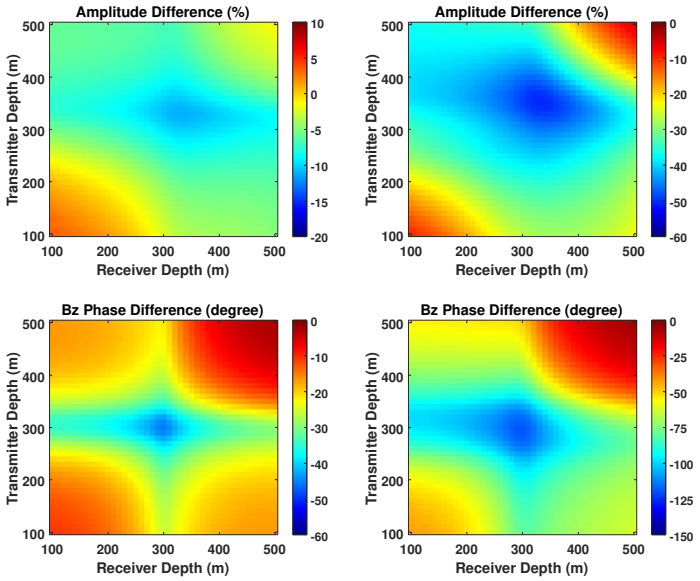
Figure 3. Cross-well EM inversion. (a) The xz cross-section at y = 0 m at T1. (b) The yz cross-section at x = 0 m at T1. (c) The xz cross-section at y = 0 m at T2. (d) The yz cross-section at x = 0 m at T2. The left column shows the true resistivity models along with the cross-well EM configuration, and the right column shows the inversion results. The white circles along the

vertical line at position = 0 m indicate source positions, and the circles at positions x= -500 m and 500 m indicate receiver positions.



(a) (b) (c)

Figure 4. Crosswell EM forward modeling data for the xz cross-sectional models. (a) T0. (b) T1. (c) T2. The first row shows the amplitude of the vertical magnetic field (Bz) and the second row shows their phase. The source well is at the center of the model (i.e., x=0m) and the receiver well at x=500m.



(a) (b)

Figure 5. Difference (a) between T0 and T1 model responses and (b) between T0 and T2 model responses. The first row shows the relative amplitude difference (%) of the vertical magnetic field (Bz) and the second row shows their phase difference (degree).

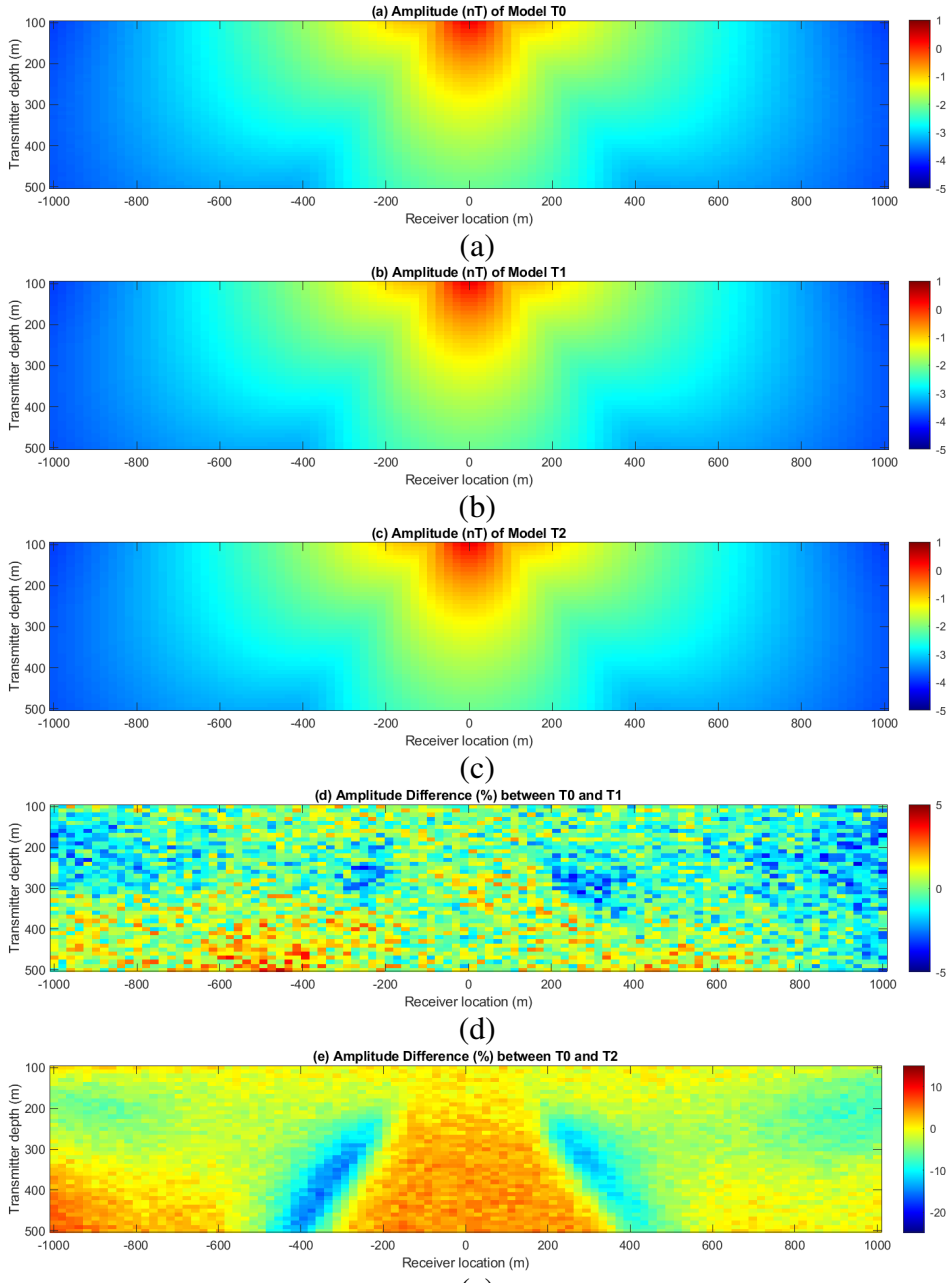


Figure 6. The borehole-to-surface EM amplitude data and relative difference (%) between T0, T1 and T2 models.

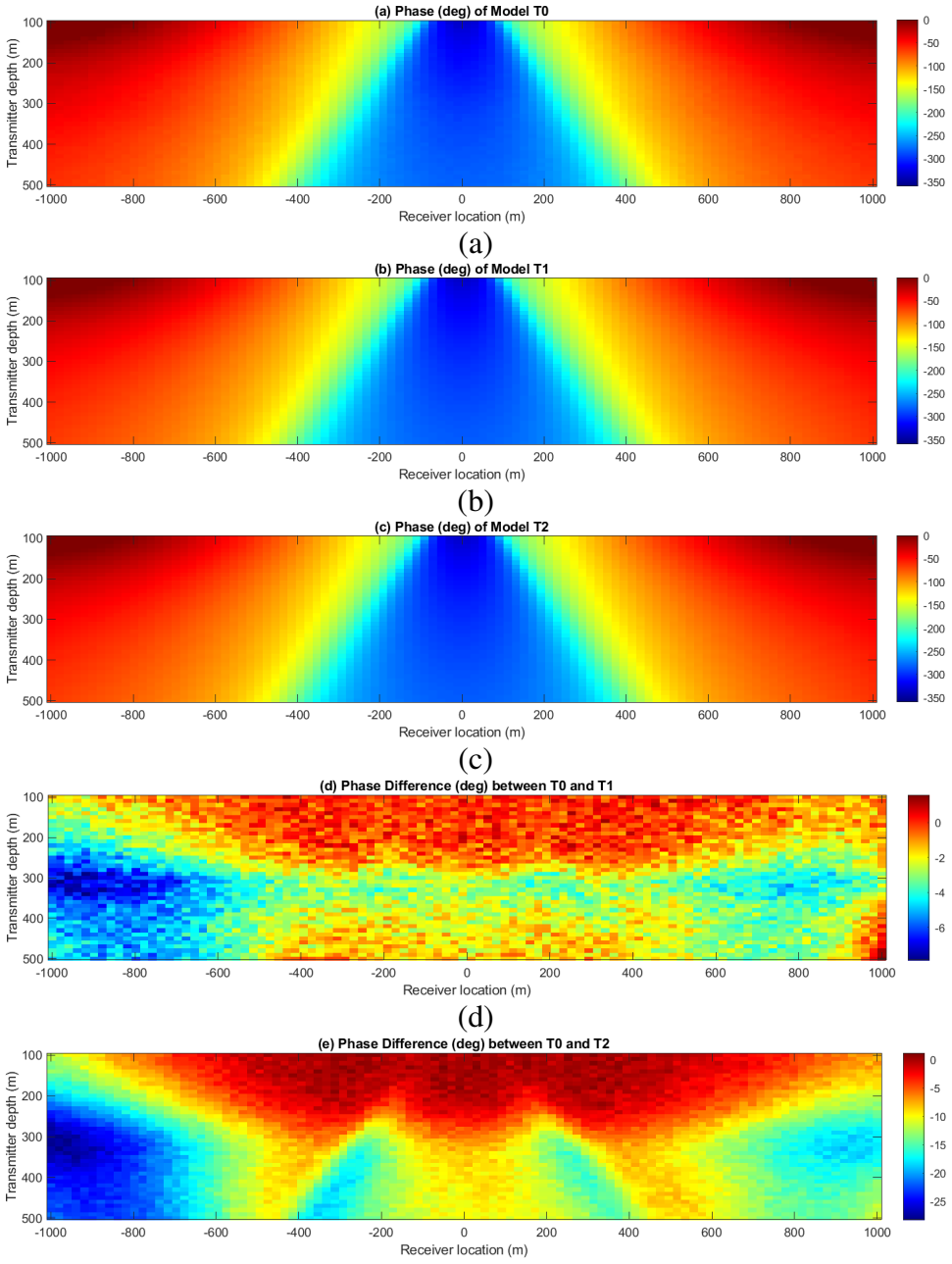
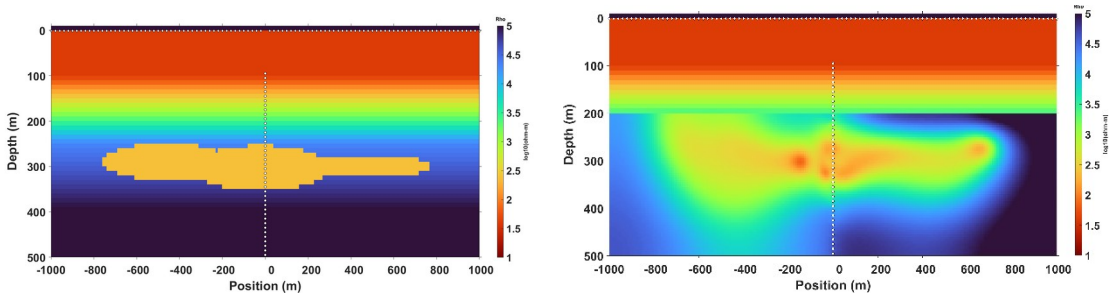
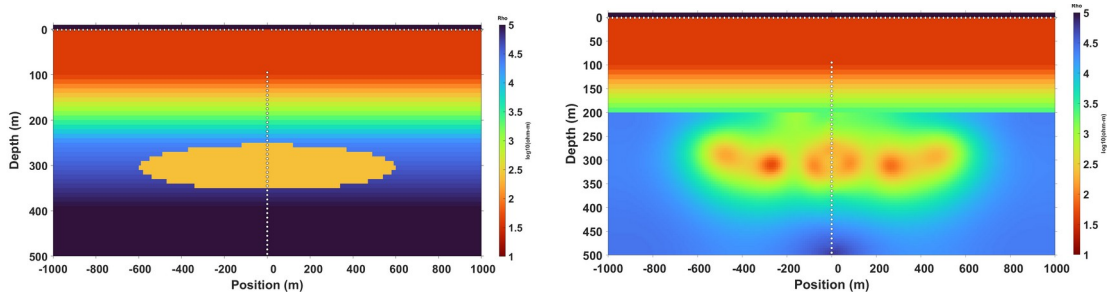


Figure 7. The borehole-to-surface EM phase data and difference (degree) between T0, T1 and T2 models.



(a)



(b)

Figure 8. Borehole-to-surface EM inversion. (a) The xz cross-section at y = 0 m at T2. (b) The yz cross-section at x = 0 m at T2. The left column shows the true resistivity models along with the cross-well EM configuration, and the right column shows the inversion results. The white circles along the vertical line at position = 0 m indicate source positions, and the circles on the surface indicate receiver positions.

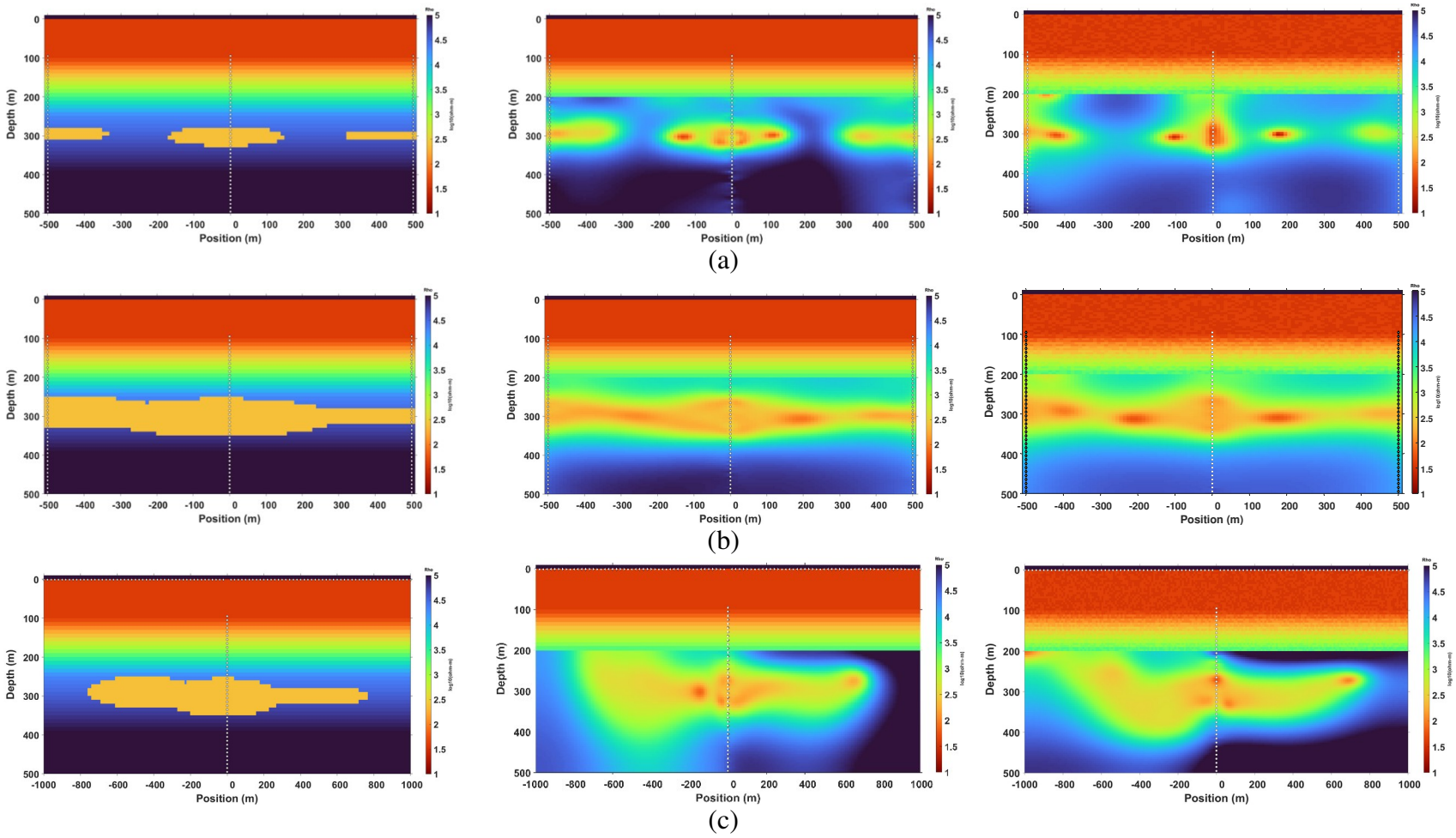


Figure 9. Comparison of the borehole EM inversion results derived using unperturbed and perturbed layered background starting models. Columns show the true resistivity models (left), inversions using the unperturbed starting model (middle), and inversions using the randomly perturbed starting model (right). All panels display xz cross-sections at y = 0 m for (a) cross-well EM at T1, (b) cross-well EM at T2, and (c) borehole-to-surface EM at T2.